9-1-2008

Inter-frequency Bias Estimation for the GPS Monitor Station Network

Donny Holaschutz
Booz Allen Hamilton

Robert H. Bishop
Marquette University, robert.bishop@marquette.edu

R. Benjamin Harris
University of Texas at Austin

Brian Tolman
University of Texas at Austin

Published version. Published as part of the proceedings of the conference, *21st International Technical Meeting of the Satellite Division of The Institute of Navigation (ION GNSS 2008)*, 2008: 2405-2415. Publisher Link.
The Institute of Navigation was the first publisher of this conference proceeding.
Robert Bishop was affiliated with the University of Texas at Austin at the time of publication.

Inter-frequency Bias Estimation for the GPS Monitor Station Network

Donny Holaschutz, *Booz Allen Hamilton*
Robert H. Bishop, *Department of Aerospace Engineering, The University of Texas at Austin*
R. Benjamin Harris and Brian Tolman, *Applied Research Laboratories, The University of Texas at Austin*

BIOGRAPHY

Donny Holaschutz is currently working as a Senior Consultant for Booz Allen Hamilton. Prior to Booz Allen Hamilton, he worked at Applied Research Laboratories, The University of Texas at Austin (ARL:UT). He received a B.S. in Aerospace Engineering and B.A. in Hispanic Studies from the University of Texas at Austin (UT Austin) (2004), and he received a M.S.E. in Aerospace Engineering (2007) from the same department.

Robert H. Bishop received his Ph.D. in electrical and computer engineering from Rice University (1990). He is a professor in the Department of Aerospace and Engineering and Engineering Mechanics at UT Austin. He currently holds the Joe J. King Professorship and is a Distinguished Teaching Professor. Dr. Bishop spent ten years as a practicing engineer with The MIT Charles Stark Draper Laboratory. He is a Fellow of AIAA.

R. Benjamin Harris is an Engineering Scientist at ARL:UT. He received a B.S. (1994) and Ph.D.(2008) in Aerospace Engineering at UT Austin, and an M.S. in Aeronautics and Astronautics from Stanford (2000). His research interests include orbital mechanics, GNSS modernization, multipath and software engineering.

Brian W. Tolman is a Research Scientist at ARL:UT, with over twenty years experience in GPS-related research, data analysis and software development. He holds a Ph.D. in theoretical physics from UT Austin.

ABSTRACT

The inter-frequency bias (IFB) is present in all dual frequency combinations of GPS pseudorange and carrier phase observables. It is caused by the path dependent signal delays in both the satellite and receiver. That delay can be directly measured for a space vehicle prior to launch, or for a ground based receiver prior to its being used in the field. However the bias is known to drift, and monitoring the delay estimate by direct measurement is time consuming for ground based receivers and impossible for deployed space vehicles. Hansen (2002) examined the observability of IFB through a global model of ionosphere total electron content (TEC). Variation in the receiver portion of the IFB can also be observed in receivers with antennae in a zero-baseline configuration. This is referred to as an inter-receiver bias (IRB).

In this study a Kalman filter is formulated to observe IFBs and IRBs. Process noise is used to allow the filter to track changes in the IFBs and IRBs. The filter also implements constraints to reflect the fact that a given IRB is not linearly independent of the IFBs. Because the receivers are distributed on a global scale, the Kalman filter requires a globally observable phenomenon by which to tie the IFBs. In this case ionosphere delay provides such a phenomenon.

The filter was applied to observations collected by GPS monitor stations that comprise the National Geospatial-Intelligence Agency Monitor Station Network (MSN). Each monitor station contains two geodetic quality receivers in a zero-baseline configuration and continuously collects GPS observations. The GPS observations collected by this network are used to produce both precise ephemeris and the broadcast ephemeris. GPS observations made through the network are incorporated into the GPS Master Control Station (MCS) Kalman filter of the Operational Control System (OCS) (Wiley, 2006). The Kalman filter in the OCS estimates the orbital parameters that are transmitted via the navigation message. If estimated effectively, knowledge of the receiver portion of the IFB can aid in achieving better ionosphere models.

IFBs are made observable using a global ionosphere delay model. A ninth order spherical harmonic model derived by Y.C. Chao (1997) was used in this study for ionosphere delay. Chao used this spherical harmonic model to capture

ionospheric variations that occurred over a smaller global region in his IFB estimation process. In this study a similar model was used but was verified using observations that span a global coverage.

The receiver portion of the IFB is observed precisely using the IRB. In this study error terms were introduced into the Kalman filter design to realign the IRB estimates to the IFB estimates produced for each of the two receivers in a zero baseline configuration. For a nominal epoch of measurement, there were 198 noisy measurements used each epoch to generate twelve monitor station specific IRBs. The IRB estimates showed small, decimeter level dynamic variation over the period of a day.

The quality of the IFB estimate directly affects the quality of the ionospheric model formed during the estimation process. Results verify that the filter is operating properly. The ionosphere model, though simple, demonstrates that the total electron content (TEC) peaks during local noon and is at a minimum during local night. IRB estimates are roughly constant over time and have a magnitude of less than 2.5 meters. Similar estimates are formed for the IFBs, however when processing one day of observations, the IFB estimates are less stable than those of the IRBs. Future effort will involve tuning the filter, and establishing criteria for its convergence.

INTRODUCTION

The National Geospatial-Intelligence Agency (NGA) operates a global network of GPS monitor stations referred to as the Monitor Station Network (MSN). Observations gathered from the MSN are used by the GPS Control Segment to monitor the GPS signal and to estimate an orbit and clock model for each satellite. The orbit and clock models are generated in real-time by a Kalman filter operated at the Master Control Station (MCS). The models are then packaged into the navigation message and uploaded to the constellation. The navigation message is broadcast by the constellation at a later date. Figure 1 depicts the role of the MSN in GPS operations [1].

Navigation accuracy depends on the accuracy inherent in the orbit and clock models available to the navigation user. For users of the navigation message, the accuracy of those models is defined in part by the accuracy of the available range measurements at the MCS. Systematic errors in range measurements can cause systematic model errors. One form of systematic error is a constant, often referred to as a *bias*. The purpose of this investigation is to develop a process that estimates the bias associated with dual frequency receivers used within the MSN, known as the inter-frequency bias (IFB). That process will not only provide an estimate but update that estimate over time as new observations are collected. Because the IFB drifts unpredictably, the estimation process must accommodate evolution in the IFB. The long term goal is to monitor the IFB in real-time.

THEORY AND BACKGROUND

The inter-frequency bias or IFB is caused by *path dependent* delay of the GPS signal between the satellite-based emitter and receiver. Furthermore, each carrier band–L1 at 1575.42 MHz and L2 at 1227.60 MHz–is processed by a unique chain of electronics or *channel* at both the emitter and receiver. An IFB is in general the difference in hardware delays between two channels tracking the same emitter. As concluded by Hansen [2], there are two ways to estimate such a bias:

1. By manufacturing a device that could directly measure the bias for each receiver and satellite in real time.
2. By fitting a model to the true ionosphere and filter the measurements through the model to separate the ionospheric delay from the hardware bias.

The latter approach will be used in this investigation because it can be implemented in software and is operationally feasible.

Ionospheric Thin Shell Model

The true ionosphere is a three dimensional space region through which all GPS signals travel. There is a characteristic total electron content (TEC) for each possible travel path of each particular GPS signal. The variation in the ionosphere causes a path delay on the range measurements as follows

$$I_{range\,delay} = \frac{40.3}{f^2} \int N_e \, d\rho. \qquad (1)$$

When the ionosphere is represented using a thin shell model, variations of the ionosphere can be described using one degree of freedom in the zenith direction. The ionosphere delay at a given location can be represented with one value, corresponding to zenith delay, for all points on the surface of the shell. As illustrated in Figure 2, all free electrons are concentrated on a spherical shell with a radius that has the length of the radius of the Earth plus the mean value of the ionospheric height, h_m. The ionospheric pierce point (IPP) is where the line of sight between the GPS receiver and GPS satellite intersects the thin shell. Accepted values for the h_m are in the 300 to 400 (km) range. Due to the geometry, the value of h_m will only affect the integration of observations made by satellites at low elevations [3].

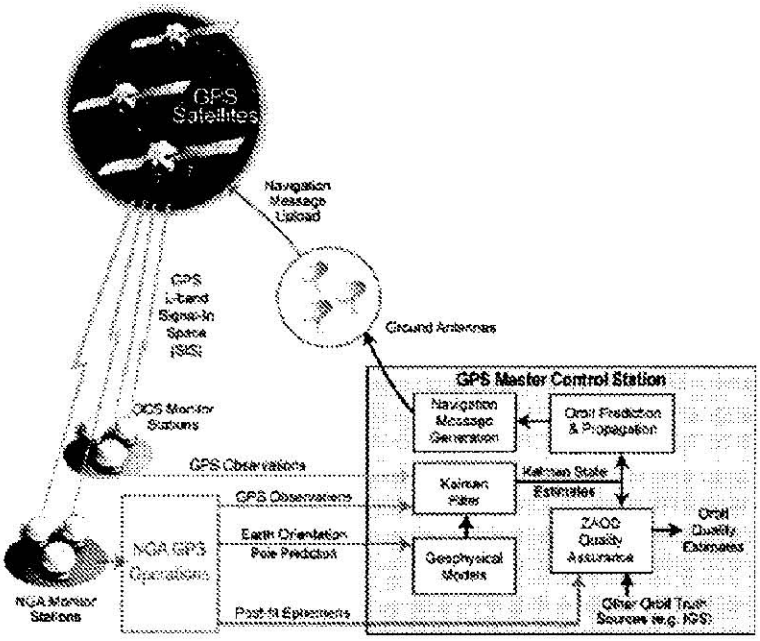

Fig. 1 Role of observations collected by the MSN in GPS operations. Image courtesy Brent Renfro, ARL:UT.

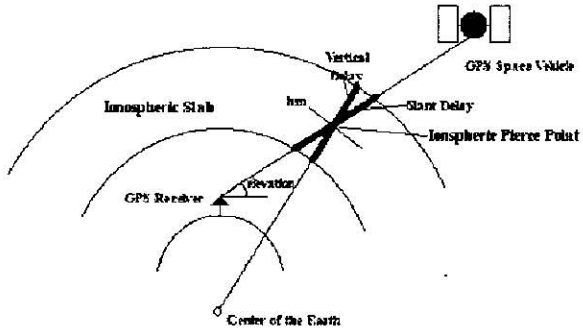

Fig. 2 Thin Shell Ionospheric Model with Vertical and Slant Delays.

The actual delay seen by a receiver is a function of relative geometry and zenith delay. For thin shell models the obliquity factor OF is defined as the ratio of slant to vertical delay. In this study, the elevation ϵ was used to compute OF as prescribed by Chao [4]:

$$OF = \sec\left[\sin^{-1}\left(\frac{R_e}{R_e + h_m}\cos\epsilon\right)\right] \qquad (2)$$

The ionospheric delay I_v, can be separated from the IFB, by concurrently estimating both the model parameters for the ionosphere and the biases. Following Chao [4], for this investigation the ionosphere will be modeled as a thin shell and the vertical variation of the thin shell model (shown in Figure 2) will be modeled using a second order spherical harmonic expansion. The vertical ionospheric delay I_v can be expressed as

$$I_v = \sum_{n=0}^{2}\sum_{m=0}^{n}[C_{nm}\cos(m\lambda_p) + S_{nm}\sin(m\lambda_p)]P_{nm}\sin(\phi_p) \qquad (3)$$

where ϕ_p is the geodetic latitude, λ_p is the longitude of the pierce points [4] . The order of the terms is noted with n, and degree with m.

The state of the ionosphere is driven by solar activity and changes in the geomagnetic field of the Earth. In the sun-earth reference frame the ionospheric vertical delay I_v varies slowly as a function of time. The vertical delay represented by the spherical harmonic model presented in Equation 3 is a function of the ionospheric pierce points. To take advantage of the slow variations of the ionosphere in the Sun-Earth (SE) reference frame, the final form of the IPP's must be defined in a frame aligned with the SE reference frame.

The MSN reference network has a global, yet sparse coverage. The geometric repetitiveness of the satellite tracks and the sparsely located monitor stations severely limit the ionospheric coverage of the network. The latitude and longitude of IPPs (ϕ_p, λ_p) are initially computed from several

station specific parameters such as station location and location of the satellite in the Earth-Centered, Earth-Fixed (ECEF) reference frame. The IPPs are sequentially converted from the ECEF frame (ϕ_p, λ_p) to the Sun-Earth (SE) frame (ϕ_{p-SE}, λ_{p-SE}).

The center of the SE reference frame is fixed at the center of the Earth, as seen in Figure 3. Z_{SE} is aligned with the ECEF z-axis which by definition aligns with the Earth's axis of rotation. The $X - Z_{SE}$ plane contains the Sun at all times, and the X_{SE} axis is oriented toward the Sun.

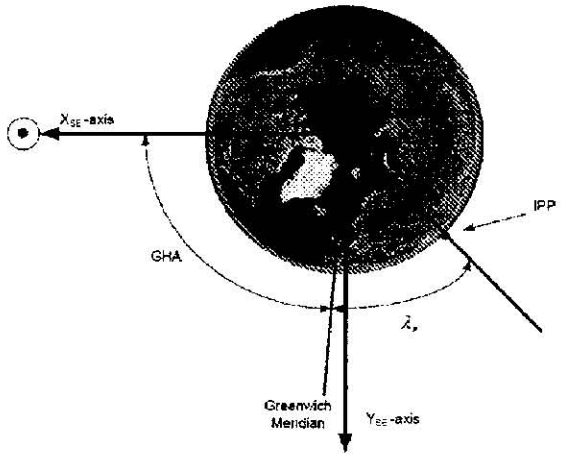

Fig. 3 Sun-Earth reference frame, with X_{SE} pointing towards the Sun.

The X_{SE} of the SE reference frame is separated by the Greenwich Hour Angle (GHA) from the intersection line created by the equatorial plane and the Greenwich Meridian plane. The ECEF IPP longitude λ_p can be transformed from the ECEF reference frame to the SE reference frame by

$$\lambda_{p-SE} = \lambda_p + GHA \tag{4}$$

where

$$GHA = \omega_{earth}(t_{UTCofGM} - t_{noon}). \tag{5}$$

The rate of rotation of the Earth, ω_{earth}, is $\frac{one\ revolution}{day}$ and $t_{UTCofGM}$ is the UTC time at the Greenwich Meridian. Since the plane formed by the X_{SE} and Y_{SE} axis span the same (equatorial) plane as the X_{ECEF} and Y_{ECEF} axes, it follows that

$$\phi_{p-SE} = \phi_p. \tag{6}$$

Inter-frequency Bias (IFB)

The satellite portion of the inter-frequency bias T^j_{gd} is defined in the IS-GPS-200 as the mean group delay differential [5]. According to the IS-GPS-200, the Control Segment assures the T^j_{gd} cancels when differencing the ranges in the ionospheric free combination by monitoring timing on the GPS satellite constellation. The receiver component of the inter-frequency bias R_i is only present in the pseudorange measurement of the L2 frequency. The receiver component of the inter-frequency bias on the L1 signal by definition is zero, because the time used by GPS receiver comes from the L1 C/A code. The multipath effects M_{PR} and noise effects E_{PR} are receiver are site dependent [4]. The pseudorange measurements on L1 and L2 are defined as

$$\tilde{PR}^j_{i\,L1} = \bar{\rho} + I_{L1} + T^j_{gd} + M_{PR1} + E_{PR1}, \tag{7}$$

and

$$\tilde{PR}^j_{i\,L2} = \bar{\rho} + I_{L2} + \gamma \cdot T^j_{gd} + R_i + M_{PR2} + E_{PR2}. \tag{8}$$

where $\bar{\rho}$ are delay terms common to both measurements, I is the ionosphere delay, and γ represents the approximately linear ratio between delay errors on L1 and L2.

The ionosphere delay is one amongst several error sources on the right side of Equations 7 and 8. Differencing Equation 8 from 7 cancels common terms, as such

$$\begin{aligned} \tilde{PR}^j_{i\,L2} - \tilde{PR}^j_{i\,L1} &= (\gamma-1)I_{L1} + (\gamma-1)T^j_{gd} + R_i + \\ &\quad M_{PR2} - M_{PR1} + \\ &\quad E_{PR2} - E_{PR1}. \end{aligned} \tag{9}$$

Dividing Equation 9 by $(\gamma - 1)$, it follows that

$$\begin{aligned} \frac{\tilde{PR}^j_{i\,L2} - \tilde{PR}^j_{i\,L1}}{\gamma-1} &= I_{L1} + T^j_{gd} + \frac{R_i}{\gamma-1} \\ &\quad + \frac{M_{PR2} - M_{PR1}}{\gamma-1} \\ &\quad + \frac{E_{PR2} - E_{PR1}}{\gamma-1}. \end{aligned} \tag{10}$$

The ionospheric range measurement $\tilde{I}_{L1}$ for L1 is defined as

$$\tilde{I}_{L1} = \frac{\tilde{PR}^j_{i\,L2} - \tilde{PR}^j_{i\,L1}}{\gamma-1}. \tag{11}$$

From Equation 11 the total inter-frequency bias including both satellite and receiver components is defined as:

$$IFB^j_i \equiv T^j_{gd} + \frac{R_i}{\gamma-1}. \tag{12}$$

The ionospheric measurement range equation can be reduced to

$$\tilde{I}_{L1} = I_{L1} + IFB^j_i + v_{PR}, \tag{13}$$

where the pseudorange noise v_{PR} can be combined to form

$$v_{PR} = \frac{M_{PR2} - M_{PR1}}{\gamma-1} + \frac{E_{PR2} - E_{PR1}}{\gamma-1}. \tag{14}$$

Inter-Receiver Bias (IRB)

The IRB measurement is a direct by-product of double observation differences performed in the zero-baseline configuration available throughout the MSN. Unlike the IFB the IRB can be directly observed without modeling the ionospheric delay, because when differencing the difference of the ranges, the ionospheric delay term is eliminated. The physical explanation follows from the correlation between signal path and ionospheric range delay described in Equation 1. Both frequency signals measured by each receiver have the same TEC because in a zero-baseline configuration they travel through the same path to get to the receiver shared antenna. The observation equation for the IRB is derived from the double difference of the range measurements as

$$\tilde{IRB}_i^j = (\tilde{PR}_{iL2}^j - \tilde{PR}_{iL1}^j)_s - (\tilde{PR}_{iL2}^j - \tilde{PR}_{iL1}^j)_u, \quad (15)$$

where s represents the selected receiver and u the unselected receiver. Traditionally, at each monitor station one of the receivers acts as the principal (which is known as the selected receiver) and the other as the backup (or unselected receiver). The IRB as defined in Equation 15 relates to known errors as follows:

$$\begin{aligned} \tilde{IRB}_i^j &= R_{si} - R_{ui} \\ &+(M_{PR2} - M_{PR1})_s - (M_{PR2} - M_{PR1})_u \\ &+(E_{PR2} - E_{PR1})_s - (E_{PR2} - E_{PR1})_u \end{aligned} \quad (16)$$

where R_{si} is the receiver bias for the selected receiver and R_{ui} is the receiver bias for the unselected receiver. The variable i corresponds to a particular monitor station in the MSN. Satellite number is noted with the j superscript. There is a multipath error M and receiver noise error E for each particular frequency and receiver. The IRB is defined as the difference between the receiver bias for the selected R_{si} and the receiver bias for the unselected R_{ui}, as is given by

$$IRB_i = R_{si} - R_{ui}. \quad (17)$$

Multipath is an error caused by the spatial reflection and refraction of the GPS signal. In a zero baseline configuration where both receivers are tethered to the same antenna the multipath difference between the receivers is

$$M_{PR1u} - M_{PR1s} = 0 \quad (18)$$

and

$$M_{PR2s} - M_{PR2u} = 0. \quad (19)$$

Thus combining all multipath and noise terms into a single noise term, we find

$$v_{IRBi} = (E_{PR2} - E_{PR1})_s - (E_{PR2} - E_{PR1})_u. \quad (20)$$

Using Equations 18 through 20, it follows that Equation 16 reduces to

$$\tilde{IRB}_i^j = IRB_i + v_{IRBi}. \quad (21)$$

Both terms on the right hand side of Equation 21 are receiver dependent. There are no terms that contain the satellite pointer j. Yet on the left side of Equation 21 the IRB is defined as i monitor station and satellite j dependent. The reason behind such phenomena is that the IRB measurement is derived from measurements that are satellite and monitor station dependent, therefore in order for a measurement to exist there must be a satellite in the line of sight of the receiver.

METHODOLOGY

Estimation System

In the estimation process, observations collected by the GPS MSN were used. The observations are stored in RINEX. The GPS Toolkit (GPSTk) open source library was used to parse the RINEX files, compute station/satellite geometry, and store those values in a MATLAB readable format [6]. The GPSTk is a suite of applications and open source library sponsored by the Space and Geophysics Laboratory at Applied Research Laboratories at the University of Texas at Austin. The data flow of the estimation process is depicted in Figure 4.

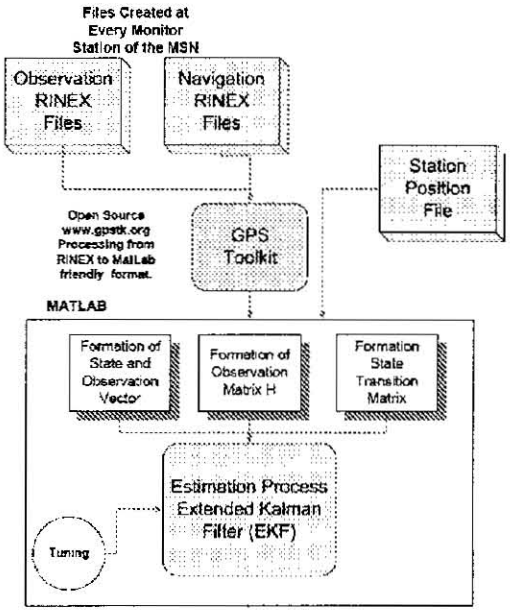

Fig. 4 Schematic of system architecture

Once all observations are in a MATLAB readable format, the state-space components are formed. These components

are the observation vector, the observation matrix, the initial state estimate and the state transition matrix. The states space components are used by the EKF algorithm which produces the state estimates. The final product in the estimation process are the IFB estimates, the IRB estimates, and the ionospheric model parameter estimates. From these final products, it is possible to obtain an unbiased estimate of the ionospheric delay.

State Space Representation

The dynamics of a linear system can be expressed by the following first-order differential equation

$$\dot{\mathbf{x}}(t) = \mathbf{A}(t)\mathbf{x}(t) + \mathbf{G}(t)\mathbf{w}(t) \tag{22}$$

where $\mathbf{x}(t)$ is the state vector of the system and $\mathbf{w}(t)$ is the measurement noise vector. The states of a dynamic system can be chosen such that they are sufficient to completely describe the unforced motion of the system of interest [7]. For the IFB estimation system, the state vector is defined as

$$\mathbf{x}(t) = \begin{bmatrix} C_{00} \\ C_{10} \\ C_{11} \\ S_{11} \\ C_{20} \\ C_{21} \\ S_{21} \\ C_{22} \\ S_{22} \\ IFB_{s_{i=1}}^{j=1} \\ \downarrow \\ IFB_{s_{i=St}}^{j=SV} \\ IFB_{u_{i=1}}^{j=1} \\ \downarrow \\ IFB_{u_{i=St}}^{j=SV} \\ IRB_{i=1} \\ \downarrow \\ IRB_{i=SV} \\ e_{i=1}^{j=1} \\ \downarrow \\ e_{i=St}^{j=SV} \end{bmatrix} \tag{23}$$

where SV is the number of active satellites in the GPS constellation and St is the number of monitor stations used over the observation period. The first nine states are the number spherical harmonic coefficients ($NSHC$) of the spherical harmonic model associated with the vertical ionospheric delay model. The next ($SV \times St$) states are the IFB_ss for the selected receiver for all possible satellite j and monitor station i combinations. Next in the state vector are the ($SV \times St$) unselected states IFB_us for all possible satellite j and monitor station i combinations. There is an IRB state for each monitor station i. Then there are ($SV \times St$) error state e_i^j combinations. The size of the state vector is n where

$$n = NSHC + St \times SV + St \times SV + St + St \times SV. \tag{24}$$

The elements of the state vector are modeled as constants. There is assumed to be no process noise correlation between the states and the process noise matrix is modeled as time invariant matrix. According to Gelb [7], a random walk process results when uncorrelated signals are integrated. The IRB, IFB and spherical harmonic coefficients can be modeled with random walk dynamics. The first members of the state are spherical harmonic coefficients for the global ionosphere delay model. The dynamics of the spherical harmonic coefficients are

$$\begin{aligned} C_{00k} &= C_{00k-1} + w_{1k-1} \\ C_{10k} &= C_{10k-1} + w_{2k-1} \\ C_{11k} &= C_{11k-1} + w_{3k-1} \\ S_{11k} &= S_{11k-1} + w_{4k-1} \\ C_{20k} &= C_{20k-1} + w_{5k-1} \\ C_{21k} &= C_{21k-1} + w_{6k-1} \\ S_{21k} &= S_{21k-1} + w_{7k-1} \\ C_{22k} &= C_{22k-1} + w_{8k-1} \\ S_{22k} &= S_{22k-1} + w_{9k-1} \end{aligned} \tag{25}$$

The process noise for the IFBs and IRBs is similar to the spherical harmonic coefficients. The IFB model for both the selected and unselected receivers is

$$IFB_{i\,k}^{j} = IFB_{i\,k-1}^{j} + w_{i\,k-1}^{j}, \tag{26}$$

where there are ($SV \times St$) number of equations for the IFBs of the selected receiver and ($SV \times St$) number of equations for the IFBs of the unselected receiver. The IRB model is

$$IRB_{ik} = IRB_{ik-1} + w_{ik-1}, \tag{27}$$

where there are St equations, one for each IRB at each monitor station.

From the definition in Equation 12, the IFB is given by

$$IFB_{i\,s}^{j} = T_{gd}^{j} + \frac{R_{si}}{\gamma - 1} \tag{28}$$

for the selected receiver, and

$$IFB_{i\,u}^{j} = T_{gd}^{j} + \frac{R_{ui}}{\gamma - 1} \tag{29}$$

for the unselected receiver. The IRB was defined by Equation 17 as

$$IRB_{i}^{j} = R_{si} - R_{ui}. \tag{30}$$

From Equations, 28, 29, and 31 the constraint equation is found to be

$$IRB_{i}^{j} - \frac{(IFB_{i\,s}^{j} - IFB_{i\,u}^{j})}{(\gamma - 1)} = 0. \tag{31}$$

The constraint that the IRBs and IFBs are linearly related must be satisfied. The constraint takes the form of a dynamic equation error defined as

$$e_{i\,k}^{j} = e_{i\,k-1}^{j} \tag{32}$$

where there are $(SV \times St)$ equations and no process noise. The lack of noise satisfies the dependency constraint. Combining Equations 31 and 32, the error state transition model is

$$e^j_{i\,k} = e^j_{i\,k-1} + IRB^j_{i\,k-1} - \frac{(IFB^j_{i\,s_{k-1}} - IFB^j_{i\,u_{k-1}})}{(\gamma - 1)}. \tag{33}$$

There are as many dynamic transition equations as there are states. These discrete dynamic transition equations can be put into matrix form,

$$\mathbf{x}_k = \mathbf{\Phi}\mathbf{x}_{k-1} + \mathbf{w}_{k-1} \tag{34}$$

where $\mathbf{\Phi}$ is known as the state transition matrix, $E[\mathbf{w}_k] = 0$ and $E[\mathbf{w}_k\mathbf{w}_j^T] = \mathbf{Q}_k\delta_{kj}$, where $\delta_{kj} = 1$ when $k = j$ and $\delta_{kj} = 0$ when $k \neq j$. Using Equations 25, 26, 27, and 33 and the definition of the state vector in equation 23, the following state transition matrix is formed

$$\mathbf{\Phi_A} = \begin{bmatrix} \mathbf{\Phi_1} & \mathbf{\Phi_2} \end{bmatrix} \tag{35}$$

$$\mathbf{\Phi_B} = \begin{bmatrix} \mathbf{\Phi_3} & \mathbf{\Phi_4} & \mathbf{\Phi_5} & \mathbf{\Phi_6} & \mathbf{\Phi_7} \end{bmatrix} \tag{36}$$

$$\mathbf{\Phi} = \begin{bmatrix} \mathbf{\Phi_A} \\ \mathbf{\Phi_B} \end{bmatrix} \tag{37}$$

where $\mathbf{\Phi}$ is a square matrix of size $n \times n$. The process noise vector is fully populated except for the last $SV \times St$ values (because Equation set 33 does not have any process noise). The state transition matrix can be partitioned into seven smaller matrices as seen in Equation 37. The seven sub-matrices are:

$$\mathbf{\Phi_1} = \mathbf{I}_{(NSHC+2\cdot SV\cdot St+St)\times(NSHC+2\cdot SV\cdot St+St)}, \tag{38}$$

$$\mathbf{\Phi_2} = 0_{(NSHC+2\cdot SV\cdot St+St)\times(SV\cdot St)}, \tag{39}$$

$$\mathbf{\Phi_3} = 0_{(SV\cdot St)\times(NSHC)}, \tag{40}$$

$$\mathbf{\Phi_4} = -(\gamma - 1)\cdot\mathbf{I}_{(SV\cdot St)\times(SV\cdot St)}, \tag{41}$$

$$\mathbf{\Phi_5} = (\gamma - 1)\cdot\mathbf{I}_{(SV\cdot St)\times(SV\cdot St)}, \tag{42}$$

$$\mathbf{\Phi_6} = \begin{bmatrix} \mathbf{I}_{(St)\times(St)} \\ \downarrow \\ \text{for all St's} \end{bmatrix}, \tag{43}$$

and

$$\mathbf{\Phi_7} = \mathbf{I}_{(SV\cdot St)\times(SV\cdot St)}. \tag{44}$$

System Observation Equations

A linear observer with measurement noise is such that it can be expressed in a discrete-time form as

$$\mathbf{z}_k = \mathbf{H}_k\mathbf{x}_k + \mathbf{v}_k. \tag{45}$$

where $\mathbf{z}_k$ is the $(m\times 1)$ measurement vector , $\mathbf{v}_k$ is the $(m\times 1)$ measurement noise vector, $\mathbf{H}_k$ is the $(m\times n)$ observation matrix that relates the state to the measurement, $E[\mathbf{v}_k] = 0$ and $E[\mathbf{v}_k\mathbf{v}_j^T] = \mathbf{R}_k\delta_{kj}$, where $\delta_{kj} = 1$ when $k = j$ and $\delta_{kj} = 0$ when $k \neq j$ [7].

The observation vector in this application is defined to be

$$\mathbf{z}_k = \begin{bmatrix} \tilde{I}_{s_{i=1}}^{j=1} \\ \downarrow \\ \tilde{I}_{s_{i=St}}^{j=SV} \\ \tilde{I}_{u_{i=1}}^{j=1} \\ \downarrow \\ \tilde{I}_{u_{i=St}}^{j=SV} \\ I\tilde{R}B_{i=1}^{j=1} \\ \downarrow \\ I\tilde{R}B_{i=St}^{j=SV} \\ \tilde{e}_{i=1}^{j=1} \\ \downarrow \\ \tilde{e}_{i=St}^{j=SV} \end{bmatrix}, \tag{46}$$

where

$$m = 4\cdot St \times SV. \tag{47}$$

The observation matrix is formed utilizing the definition of the state vector, the observation vector and the observation equations, as

$$\tilde{I}_{L1} = I_{L1} + IFB_i^j + v_{PR_i^j}, \tag{48}$$

where the ionospheric delay I_{L1} is defined by

$$\begin{aligned} I_{L1} &= OF(I_v) \\ &= OF(C_{00} + C_{10}\sin(\phi_p) + C_{11}\cos(\lambda_p)\cos(\phi_p) \\ &\quad + S_{11}\sin(\lambda_p)\cos(\phi_p) + \tfrac{1}{2}C_{20}(3\sin^2(\phi_p) - 1) \\ &\quad + 3C_{21}\cos(\lambda_p)\sin(\phi_p)\cos(\phi_p) \\ &\quad + 3S_{21}\sin(\lambda_p)\sin(\phi_p)\cos(\phi_p) \\ &\quad + 3C_{22}\cos(2\lambda_p)\cos^2(\phi_p) \\ &\quad + 3S_{22}\sin(2\lambda_p)\cos^2(\phi_p)), \end{aligned} \tag{49}$$

$$I\tilde{R}B_i^j = IRB_i + v_{IRBi}, \tag{50}$$

and

$$\tilde{e}_i^j = e_i^j. \tag{51}$$

The observation matrix can be partitioned into nine sub-matrices:

$$\mathbf{H} = \begin{bmatrix} \mathbf{H}_1 & \mathbf{H}_2 & \mathbf{H}_3 \\ \mathbf{H}_4 & \mathbf{H}_5 & \mathbf{H}_6 \\ \mathbf{H}_7 & \mathbf{H}_8 & \mathbf{H}_9 \end{bmatrix}. \tag{52}$$

The first of the nine submatrices that comprise $\mathbf{H}$ is:

$$\mathbf{H}_1 = [\mathbf{h_1} \rightarrow \mathbf{h_q} \rightarrow \mathbf{h}_{SV \cdot St}\, \mathbf{h_1} \rightarrow \mathbf{h_q} \rightarrow \mathbf{h}_{SV \cdot St}]^T \quad (53)$$

where $\mathbf{h}_q$ is a row vector containing information about each potential pierce point q:

$$\mathbf{h}_q = OF_q a_q \begin{bmatrix} 1 \\ \sin\phi_q \\ \cos\lambda_q \cos\phi_q \\ \sin\lambda_q \cos\phi_q \\ \frac{3}{2}(\sin^2\phi_q - 1) \\ 3\cos\lambda_q \sin\phi_q \cos\phi_q \\ 3\sin\lambda_q \sin\phi_q \cos\phi_q \\ 3\cos 2\lambda_q \cos^2\phi_q \\ 3\sin 2\lambda_q \cos^2\phi_q \end{bmatrix}^T$$

The scalar a_q is a gating function that defines visibility between satellites j and station i. When there is no visibility, $a_q = 0$; when there is, $a_q = 1$. As satellite/station geometry changes over time, the value of a_q changes as well.

The variable q acts as an index of all possible combinations of satellites and stations. The mapping is as follows. The range of q is from one to $SV \cdot St$. Each value represents a combination of single station and satellite. For $q = 1$, the station number is 1 and satellite is 1. For $q = 2$, the station is still 1 but the satellite number is incremented to 2. The mapping for higher q values continues similarly until the maximum number of satellites has been assigned, in which case the satellite mapping resets to 1 and the station number is incremented to 2. Note that the absence of a given satellite for the whole day causes $\mathbf{H}$ to have deficient rank.

The remainder of the nine submatrices that comprise $\mathbf{H}$ are defined as follows:

$$\mathbf{H_2} = diag(\begin{bmatrix} a_1 \\ \downarrow \\ a_q \\ \downarrow \\ a_{SV \cdot St} \\ a_1 \\ \downarrow \\ a_q \\ \downarrow \\ a_{SV \cdot St} \end{bmatrix}), \quad (54)$$

$$\mathbf{H_3} = 0_{(2 \cdot SV \cdot St) \times (St + SV \cdot St)}, \quad (55)$$

$$\mathbf{H_4} = 0_{(SV \cdot St) \times (NSHC + 2 \cdot SV \cdot St)}, \quad (56)$$

$$\mathbf{H_5} = \begin{bmatrix} diag([\ b_{11} \rightarrow b_{1j}\ ]) \\ \downarrow \\ diag([\ b_{i1} \rightarrow b_{ij}\ ]) \\ \downarrow \\ \text{for all } i's \end{bmatrix}, \quad (57)$$

$$\mathbf{H_6} = 0_{(SV \cdot St) \times (SV \cdot St)}, \quad (58)$$

$$\mathbf{H_7} = 0_{(SV \cdot St) \times (SV \cdot St + NHSC)}, \quad (59)$$

$$\mathbf{H_8} = 0_{(SV \cdot St) \times (SV \cdot St + St)}, \quad (60)$$

and

$$\mathbf{H_9} = 0_{(SV \cdot St) \times (SV \cdot St)}. \quad (61)$$

The scalar b_{ij} is a gating function that defines visibility between satellites j and station i. When there exists no visibility $b_{ij} = 0$ and when there is visibility $b_{ij} = 1$.

Processing

The Extended Kalman Filter (EKF) has the capability of producing estimates for a process which has non-linear dynamics or measurement relationship. The dynamics for the IFB estimation problem are linear, but the measurement relationships are non-linear. To linearize the measurement relationships the Jacobian was used to produce a $\mathbf{H}$ matrix about the nominal solution. In the formation of the $\mathbf{H}$ matrix shown in the prior section the linearization was accounted for and the creation of the $\mathbf{H}$ matrix was shown in an algorithmic fashion. Note that the spherical harmonic terms of the observation matrix $\mathbf{H}$ are non-linear and time-varying. The IFB estimation is a discrete process since the measurements to update the states are not known continuously, but at the rate at which observation are recorded. The discrete system model whose state at time t_k is denoted by $\mathbf{x}_k$ is

$$\mathbf{x}_k = \mathbf{\Phi}_{k-1}\mathbf{x}_{k-1} + \mathbf{w}_{k-1}. \quad (62)$$

The non-linear discrete measurement model is

$$\mathbf{z}_k = \mathbf{h}(\mathbf{x}_k) + \mathbf{v}_k \quad (63)$$

where $\mathbf{w}_k$ is the process noise vector and $\mathbf{v}_k$ is the measurement noise vector. Both the measurement noise vector and process noise vector are being modeled as random variables [7]. The EKF time update equations are

$$\hat{\mathbf{x}}_k^- = \mathbf{\Phi}_{k-1}\hat{\mathbf{x}}_{k-1}^+ \quad (64)$$

and

$$\mathbf{P}_k^- = \mathbf{\Phi}_{k-1}\mathbf{P}_{k-1}^+\mathbf{\Phi}_{k-1}^T + \mathbf{Q}_{k-1} \quad (65)$$

where k is the current time step and k-1 is the previous time step, $\mathbf{\Phi}_k$ is the state transition matrix, $\mathbf{P}_{k-1}^+$ is the previous covariance matrix, and $\mathbf{Q}_{k-1}$ is the process noise. The purpose of the time update is to project the state and covariance from the previous time step to the current time step. The measurement update equations are

$$\mathbf{K}_k = \mathbf{P}_k^-\mathbf{H}_k^T(\mathbf{H}_k\mathbf{P}_k\,\mathbf{H}_k^T + \mathbf{V}_k\mathbf{R}_k\mathbf{V}_k^T)^{-1}, \quad (66)$$

$$\hat{\mathbf{x}}_k^+ = \hat{\mathbf{x}}_k^- + \mathbf{K}_k(\mathbf{z}_k - \mathbf{h}(\hat{\mathbf{x}}_k^-)), \quad (67)$$

and

$$\mathbf{P}_k^+ = (\mathbf{I} - \mathbf{K}_k\mathbf{H}_k)\mathbf{P}_k^-. \quad (68)$$

$\mathbf{H}_k$ is the observation matrix formed for the k-th time step, $\mathbf{R}_k$ is the measurement noise covariance matrix, $\mathbf{K}_k$ is the Kalman gain matrix, and $\mathbf{h}(\hat{\mathbf{x}}_k^-)$ is the observation equation evaluated at with the projected estimate of the state at the current step [8]. To achieve more accurate estimate, the Joseph algorithm was used,

$$\mathbf{P}_k^+ = (\mathbf{I} - \mathbf{K}_k\mathbf{H}_k)\mathbf{P}_k^-(\mathbf{I} - \mathbf{K}_k\mathbf{H}_k)^T + \mathbf{K}_k\mathbf{R}_k\mathbf{K}_k^T. \quad (69)$$

To initialize the time update equations in the filter an initial estimate of the covariance matrix $\mathbf{P}_o$ and state vector $\hat{\mathbf{x}}_o$ are required.

ANALYSIS

Ionospheric Estimates

The ionospheric delay measurement contains the IFB, the ionospheric delay, and noise. In the estimation process, an estimate for the IFB for each satellite receiver combination is obtained. A model for the vertical ionospheric delay is being estimated as well. The obliquity factor (OF) relates the path delay to the vertical delay. With knowledge of the OF and the estimated value of the vertical ionospheric delay one can compute an estimated path delay for a particular satellite receiver combination via

$$\hat{I}_{i\,L1}^j = OF\ \hat{I}_{v\,L1} + \hat{IFB}_i^j. \quad (70)$$

Ideally the estimated ionospheric delay should be a noise

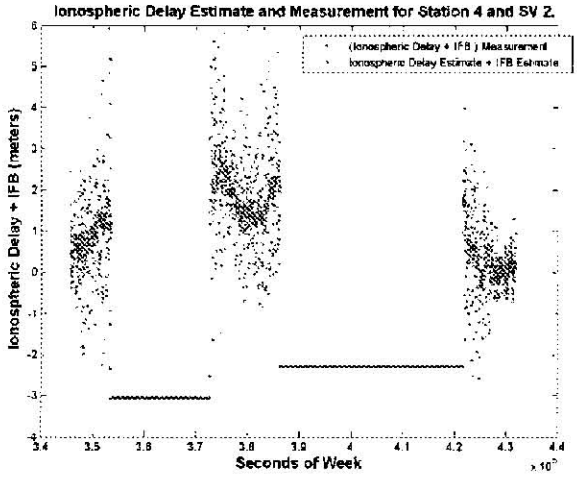

Fig. 5 Plot of the ionospheric delay measurement and ionospheric delay estimate for DOY 348 at the England Station.

free estimate of the measured ionospheric delay. Figure 5 shows the estimated and measured delays for the England Station observing space vehicle (SV) 2. At the beginning of DOY 348 the England station is tracking SV 2. A couple of hours later the satellite goes out of view from the monitor station. When the satellite is out of view, the ionospheric delay measurement which is produced from a GPS range observation combination is zero, hence no observations are being recorded. At about 3.75×10^5 seconds of week, the satellite comes back in view and an ionospheric delay measurement becomes available. In Figure 5, one can see that the ionospheric delay estimate is tracking the ionospheric measurement and the noise of the measurement is much higher than that of the estimate as expected. After the monitor station loses sight of SV 2, the filter updates a_q so that observation y_q has no impact on the state estimate. The expected ionosphere measurement is evaluated for that period, then taking the value of the IFB. Figure 5 shows verifies this expected behavior. In this example, the estimate remains consistent even after the second time the satellite comes in view. To isolate the IFB the iono-

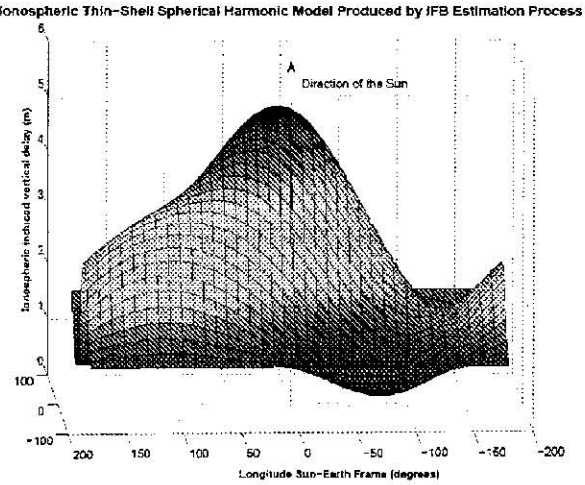

Fig. 6 The ionospheric thin-shell model generated in the estimation process in the Sun-Earth reference frame, with X_{SE} pointing towards the Sun.

spheric path delay must be removed. A thin shell model represented by spherical harmonics was used to capture the ionospheric vertical bely in the Sun-Earth frame. As seen in Figure 6 the ionospheric model generated as part of the estimation process shows a higher vertical delay $I_{v\,L1}$ in the direction of the Sun as expected. The ionospheric vertical delay has a maximum of about 5m and it has its lowest point close to the dark side of the Earth.

IFB Estimates

The purpose of the previous section was to establish the credibility of the ionospheric model being produced. As

discussed earlier, the quality of the IFB estimate depends on how well the ionospheric model is able to absorb the true path delays on the GPS signal. For the data-set presented in this section there were 696 inter-frequency bias combinations estimated. Two examples of the IFB estimate time evolution that show important features will be shown.

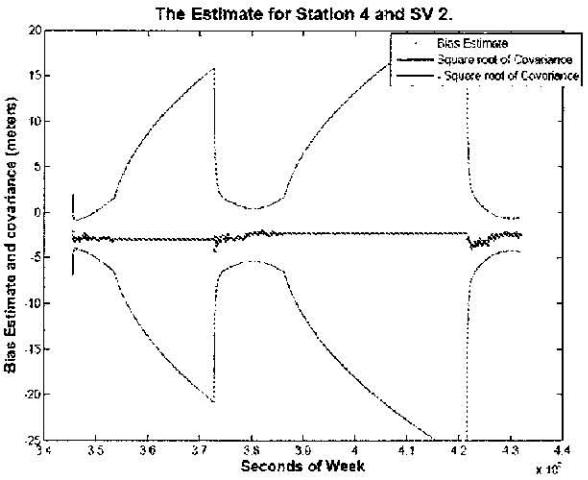

Fig. 7 Plot of the square root of the covariance and the inter-frequency bias for SV 2 on DOY 348 at the England Station.

Figure 7 shows the inter-frequency bias estimate evolution and the square-root of the covariance over time. As seen Figure 7, one of the striking aspects is the growth in the covariance when there are no ionospheric delay measurements. The ionospheric delay measurements presented in Figure 5 are being used to produce the IFB estimate in Figure 7. After the satellite goes out of sight, the uncertainty in the estimate grows because the filter does not have any measurements to update the estimate. Notice that the estimate remains at a fixed value as expected. Right before the satellite is about to come in view again, the covariance reaches a peak value, then it begins to rapidly decrease as the filter processes the available measurements. The growth in the covariance impacts the initial estimates at the beginning of the pass. After some time, the estimates begin to converge to a constant value for the IFB.

Inter-Receiver Bias Estimates

As shown in a previous section the IRB can be directly observed. There are only as many inter-receiver biases as there are active monitor stations with zero-baseline capabilities. Yet the bias can be observed over every set of satellite range observations. For the DOY 348 data set used in this results section there were 348 observations made to estimate the 12 inter-receiver biases, 29 per inter-receiver bias. The estimates of the inter-receiver biases are shown

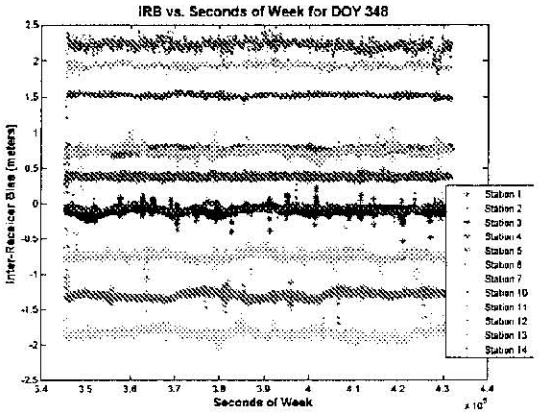

Fig. 8 Plot the IRB estimate evolution with time for MSN DOY 348.

in Figure 8. The reasons behind this dynamic variation are temperature fluctuations in the receiver or other receiver internal hardware dynamics [4].

CONCLUSIONS

The ionosphere delay model plays a very important role in the estimation of the IFBs. In order to extract the bias one must remove the ionospheric delay. A higher fidelity ionospheric model and more globally distributed ionospheric measurements would improve the inter-frequency bias estimation process.

FUTURE WORK

More than 1200 states are being estimated, leading to a large computational burden during the Kalman update. Improvements in matrix inversion techniques and more computational power will improve run times. The IRB estimates are relatively stable and constant but there are some slowly evolving dynamics associated with these biases. An accepted global convergence criteria has not been developed for the IFBs. A better understanding of these biases could improve the ephemeris generation process.

While the results presented in this paper show promise there is still room for improvement in the IFB estimation process. A convergence criteria should be established and the selected algorithm evaluated over data sets spanning longer periods of time. The ionospheric model plays a critical role in the estimation process and improving such a

model could have a positive effect on the IFB estimates. Future investigations will determine if it is possible to isolate T_{gd} from IFB and IRB estimates. Also future work will focus on demonstrating how the IFB and IRB estimates can be applied to precise point positioning, navigation and ionosphere modeling.

ACKNOWLEDGEMENTS

The authors of this paper would like to acknowledge the support received by the National Geospatial-Intelligence Agency. This investigation was completed in support of contract/task N00024-01-D-6600-5-124. The authors would also like to recognize the support received by ARL:UT and the Department of Aerospace Engineering and Engineering Mechanics Department at the University of Texas at Austin.

REFERENCES

[1] Barbara Wiley, David Craig, Dennis Manning, J. Novak, R andall Taylor, and Leonard Weingarth. NGA's Role in GPS. In *Proceedings of the 19th International Technical Meeting of the Satellite Division of the Institute of Navigation*, Fort Worth, Texas, September 2006.

[2] Andrew J. Hansen. *Tomographic Estimation of the Ionosphere using Terrestial GPS Sensors* . PhD thesis, Stanford University, March 2002.

[3] B. Hofmann-Wellenhof, H.Lichtenegger, and J. Collins. *GPS Theory and Practice*. Springer-Verlag/Wien, fifth, revised edition edition, 2001.

[4] Yi-Chung Chao. *Real Time Implementation of the Wide Area Augmentation System for the Global Positioning System with an Emphasis on Ionospheric Modeling*. PhD thesis, Standford University, 1997.

[5] LLC ARINC Engineering Services. Interface Specification IS-GPS-200, IRN-200D-001. Technical Report Revision D, GPS Joint Program Office, El Segundo, California, March 2006.

[6] Brian Tolman, R. Benjamin Harris, Tom Gaussiran, David Munton, Jon Little, Richard Mach, Scot Nelsen, ARL:UT Brent Renfro, and University of California Berkeley. David Schlossberg. The GPS Toolkit – Open Source GPS Software. In *Proceedings of the 17th International Technical Meeting of the Satellite Division of the Institute of Navigation*, Long Beach, California, September 2004. ION GNSS 2004.

[7] Arthur Gelb, Joseph F. Kasper, Jr., Raymond A. Nash, Jr., Charles Price, and Arthur A. Sutherland, Jr. *Applied Optimal Estimation*. The M.I.T. Press, 1974.

[8] Greg Welch and Gary Bishop. An Introduction to the Kalman Filter. University of North Carolina at Chapel Hill, Department of Computer Science, Chapel Hill, NC 27599-3175, 2001. SIGGRAPH.